*Regular Article*

PHYSICAL CHEMISTRY RESEARCH
Published by the
*Iranian Chemical Society*
www.physchemres.org
info@physchemres.org

***Phys. Chem. Res.**, Vol. 5, No. 2, 377-394, June 2017*
**DOI: 10.22036/pcr.2017.57688.1282**

# Modulation Response and Relative Intensity Noise Spectra in Quantum Cascade Lasers

H.H. Warid
*Physical Department, Thi-Qar University, 64001 Nasiriyah, Iraq*
*(Received 13 July 2016, Accepted 23 January 2017)*

Static properties, relatively intensity noise and intensity modulation response in quantum cascade lasers (QCLs) are studied theoretically in this paper. The present rate equations model consists of three equations for the electron density in the conduction band and one equation for photon density in cavity length. Two equations were derived to calculate the noise and modulation response. Calculations in this paper are focused on the effect of optical phonon emission rate τij, number of stages and the gain coefficient on the noise spectrum and modulation response in these types of semiconductor lasers. The results indicate the strong effect of optical phonon emission rate, gain coefficient and number of stages on the dynamics properties of QCLs. The static properties such as the population inversion, threshold injection current and steady state photon density deviate from the ideal values with increasing in $\tau_{21}$ .The effect of optical phonon emission rate $\tau_{21}$ has similar effect to that of the photon lifetime on the noise spectrum in comparison with other times.

**Keywords:** Quantum cascade lasers, Intensity noise, Intensity modulation, Rate equation model, Quantum well lasers

## INTRODUCTION

Since their first realization in 1994, the performance and frequency range of quantum cascade lasers (QCLs) are continually improving. High-performance QCLs are desired for potential applications ranging from molecular detection to telecommunications. Their narrow linewidths, large direct intensity modulation (IM) bandwidth, high output power and possible ambient temperature operation make them attractive in optical free space data communication and light detection and ranging (LIDAR) applications.

QCLs sources in the regimes 3-5 μm and 8-14 μm with high modulation bandwidths are always desirable for high-speed data transmission systems. However, the modulation bandwidth of directly modulated semiconductor laser source is largely limited by relaxation resonance frequency determined by carriers and photons lifetimes [1,2]. In recent years, the investigation of IMR and RIN of QCLs has become of utmost importance especially with the increasing need to laser sources having low noise level and large modulation bandwidth because of each of the sensitivity of absorption spectroscopy, the modulation bandwidth and the transmission range of optical free-space data links strongly limited by the intensity noise properties and modulation bandwidth of QCLs.

RIN has been investigated theoretically using rate equation model to describe the effect of the time constants of the laser dynamics on the RIN of a variety of structures [3,4]. Current modulation response of QCLs has been studied in [5]. It was found that the bandwidth of almost all QCLs is limited by the inverse photon lifetime inside the laser cavity to tens of gigahertz. On the other hand, the RIN of QCLs decreases more slowly with increasing optical output power. This is unlike the RIN behavior in interband semiconductor lasers [6,7].

In Ref. [8], the effect of a number of gain stages in the active region ($N_b$) has been studied by 3-level rate equation model. It was found that the contributions of non-radiative losses of carriers out of the upper laser level become the dominant noise source with increasing ($N_b$). Also, compared

*Corresponding author. E-mail: hussein_hade@yahoo.com

to interband semiconductor lasers, the different noise properties of QCLs originating from the effect of the short electron lifetime and the cascaded active region together.

IMR has been investigated in several theoretical works. In Ref. [9], it is found that terahertz modulation bandwidth may be achievable due to the picosecond carrier lifetimes which are characteristic of such structures. The effect of both the relevant carrier and tunneling lifetime of a prototype triple quantum well structure of IMR has been investigated through self-consistent rate equation analysis in Ref. [10]. The results indicated a correlation between the modulation bandwidth and the optical output power of the laser. Also, the maximum modulation frequency does not increase monotonically with increasing optical output power, and modulation response frequency can be obtained using device design parameters which result in a decreased photon lifetime.

In Ref. [5], it is found that QCLs have the potential for achieving terahertz dc modulation bandwidths. The IMR has been investigated using simplified rate equation to study the effect of each of fast carrier removal rates and slow carrier removal rates in Ref. [11]. For fast carrier removal rates, the results indicated that the bandwidth tends to a constant value of the order of 1000 GHz with an increase in light power. For slow carrier removal rates, a peak can be appeared in IMR at large bias currents [11]. The aim of the present contribution is to offer a theoretical description of the IMR and RIN at emitting wavelengths of 4.6 μm [6] and 9 μm [7] corresponding to the two atmospheric transmission windows, respectively, by using coupled rate equation model to describe the carrier dynamics. This paper is organized as follows. In Section 2, we present the four-level rate equation model describing the carrier dynamics in QCLs, three equations for carriers and one equation for photons. In Section 3, we perform a small signal analysis of the rate equations and derive an expression for the RIN and IMR of QCLs lasers. In section 4, numerical results are presented. Finally, section 5 gives the main conclusions.

## THEORY

To improve the performance of QCLs, it is necessary to study the crucial device parameters and how to further improve them. The crucial device parameters such as saturation photon density, threshold injection current and slope efficiency of the QCLs can be estimated using a rate equation model. QCLs consists of a several repeating structures in which each repeat unit is made up of an injector, a gain region and an injector region coupling two successive active regions and enables the electrons tunneling from an active well to higher energy level in the active region of the next period. Each gain stage incorporates three energy levels labeled |1>, |2>, and |3> with densities $N_1$, $N_2$ and $N_3$, respectively. The optical gain and the carrier dynamics inside gain region for QCLs can be considered by forming a simplified three-level model for the electrons moving through a three-level system as shown in Fig. 1.

In this model, the laser transition occurs between |3> and |2> levels. Electrons are injected into level |3> with an injection current $I_{in}$ and an injection efficiency η, where they either relax to levels |2> and |1> with a total rate $\tau_e^{-1} = \tau_{31}^{-1} + \tau_{32}^{-1}$, where $\tau_{31}$ and $\tau_{32}$ are the phonon scattering times between levels |3> and |1>, and between levels |3> and |2>, respectively. The phonon scattering times between levels |2> and |1> is $\tau_{21}$, the carriers relax into level |1> by the emission of a longitudinal-optical phonon and tunnel through the exit barrier into the subsequent miniband. All these times are dependent on two parameters; the energy difference between the corresponding states and the phonon energy of scattering process. The rate equations can be described as follows:

$$\frac{dN_3}{dt} = \eta\frac{I_{in}}{q} - \frac{N_3}{\tau_{32}} - \frac{N_3}{\tau_{31}} - \frac{G_d(1-\epsilon S)}{N_p}(N_3 - N_2)S \quad (1)$$

$$\frac{dN_2}{dt} = \frac{N_3}{\tau_{32}} - \frac{N_2}{\tau_{21}} + \frac{G_d(1-\epsilon S)}{N_p}(N_3 - N_2)S \quad (2)$$

$$\frac{dN_1}{dt} = \frac{N_3}{\tau_{31}} + \frac{N_2}{\tau_{21}} - \frac{N_1}{\tau_{out}} \quad (3)$$

$$\frac{dS}{dt} = G_d(1-\epsilon S)(N_3 - N_2)S + \frac{\beta N_3}{\tau_e} - \frac{S}{\tau_p} \quad (4)$$

where q is the electron charge, $\tau_p$ is the photon lifetime, S is

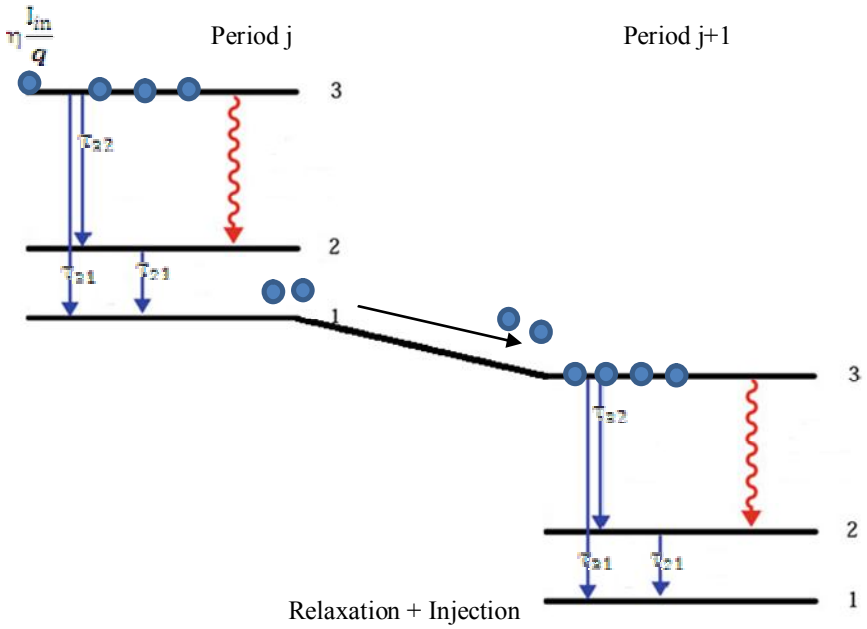


**Fig. 1.** Quantum cascade design; each repeated period consists of an active (gain) region followed by a relaxation/injection region.

the photon number, $G_d$ is the linear gain coefficient, ε is the gain compression factor, $N_p$ is the number of stages, $\tau_{out}$ is the tunneling time of carriers out of level |1> into the subsequent miniband and β is the spontaneous emission factor. Setting the left-hand side in Eqs. ((1)-(4)) to zero, the steady-state response in the three energy levels and photons' density can be written as:

$$\eta\frac{I_{in}}{q}-\frac{N_3}{\tau_{32}}-\frac{N_3}{\tau_{31}}-\frac{G_d(1-\epsilon S)}{N_p}(N_3-N_2)S=0 \tag{5}$$

$$\frac{N_3}{\tau_{32}}-\frac{N_2}{\tau_{21}}+\frac{G_d(1-\epsilon S)}{N_p}(N_3-N_2)S=0 \tag{6}$$

$$\frac{N_3}{\tau_{31}}+\frac{N_2}{\tau_{21}}-\frac{N_1}{\tau_{out}}=0 \tag{7}$$

$$G_d(1-\epsilon S)(N_3-N_2)S+\frac{\beta N_3}{\tau_e}-\frac{S}{\tau_p}=0 \tag{8}$$

Solving Eqs. ((5)-(8)), we obtain population inversion ($N_3$-$N_2$), steady state electron densities in the three energy levels, $N_{30}$, $N_{20}$, $N_{10}$ and steady state photon density $S_0$ as follows:

$$N_3-N_2=\frac{\eta\frac{I_0}{q}(1-\kappa)}{\frac{1}{\tau_e}-\frac{G_d(1-\epsilon S)}{N_p}S(1-\kappa+\rho)} \tag{9}$$

$$N_{30}=\frac{\eta\frac{I_0}{q}+\frac{G_d(1-\epsilon S_0)N_{20}S_0}{N_p}}{\frac{1}{\tau_{32}}+\frac{1}{\tau_{32}}+\frac{G_d(1-\epsilon S_0)S_0}{N_p}} \tag{10}$$

$$N_{20}=\frac{\frac{N_{30}}{\tau_{32}}+\frac{G_d(1-\epsilon S_0)N_{30}S_0}{N_p}}{\frac{1}{\tau_{21}}+\frac{G_d(1-\epsilon S_0)S_0}{N_p}} \tag{11}$$

$$N_{10}=\frac{\frac{N_{30}}{\tau_{31}}+\frac{N_{20}}{\tau_{21}}}{\frac{1}{\tau_{out}}} \tag{12}$$

$$S_0 = \frac{\frac{\beta N_{30}}{\tau_e}}{\frac{1}{\tau_p} - G_d(1-\epsilon S_0)(N_{30}-N_{20})} \quad (13)$$

where $\kappa = \tau_{21}/\tau_{32}$, $\rho = \tau_{21}/\tau_{\varepsilon}$. By following the same procedure in Ref. [11] and after simple mathematical steps, the saturation photon density $S_s$ and the threshold injection current $I_{th}$ can be written as:

$$I_{th} = \frac{q}{\eta\tau_e\tau_p G_d(1-\epsilon S)(1+\gamma)(1-\delta)} \quad (14)$$

$$S_s = \frac{N_p}{\tau_e(1+\gamma)G_d(1-\epsilon S)}\left(\frac{I}{I_{th}} - 1\right) \quad (15)$$

where $\gamma = \tau_{21}/\tau_{32}$ and $\delta = \tau_{21}/\tau_e\,(1+\gamma)$. It is clear that each of $S_s$, $(N_3\text{-}N_2)$ and $I_{th}$ depends clearly and explicitly on $\gamma$, $(\kappa,\rho)$ and $(\gamma,\delta)$, respectively, and hence on the phonon scattering time $\tau_{21}$ between levels $|2\rangle$ and $|1\rangle$. Therefore, when other parameters are constant, any increase in $\tau_{21}$ value leads to changes in static properties as in Figs. 2, 3 and 4.

## DYNAMIC MODULATION RESPONSE

To derive an expression for the IMR, we assume small deviations around the steady-state values of the photon density, and carrier density can be expressed as follows:

$$X = X_0 + \Delta X e^{j\omega t} \quad (16)$$

Where $X_0$, represents the steady-state values $N_{30}$, $N_{20}$, $N_{10}$ and $S_0$. $\Delta X$ represents the small signal deviations $\Delta n_3$, $\Delta n_2$, $\Delta n_1$, and $\Delta s$. $i_w$ represents the complex time-harmonic angular frequency. The linearized equations can be placed in matrix form:

$$\begin{vmatrix} C_{11} & C_{12} & C_{13} & C_{14} \\ C_{21} & C_{22} & C_{23} & C_{24} \\ C_{31} & C_{32} & C_{33} & C_{34} \\ C_{41} & C_{42} & C_{43} & C_{44} \end{vmatrix} \begin{vmatrix} \Delta n_3 \\ \Delta n_2 \\ \Delta n_1 \\ \Delta s \end{vmatrix} = \begin{vmatrix} 0 \\ 0 \\ 0 \\ 0 \end{vmatrix} \quad (17)$$

where the matrix terms are:

$$C_{11} = j\omega + \frac{1}{\tau_{32}} - \frac{1}{\tau_{31}} - \frac{G_d(1-\epsilon S_0)}{N_p}S_0 \quad (18a)$$

$$C_{12} = -\frac{G_d(1-\epsilon S_0)}{N_p}S_0 \quad (18b)$$

$$C_{14} = \frac{G_d(1-\epsilon S_0)}{N_p}(N_{30}-N_{20}) \quad (18c)$$

$$C_{21} = -\frac{1}{\tau_{32}} - \frac{G_d(1-\epsilon S_0)}{N_p}S_0 \quad (18d)$$

$$C_{22} = j\omega + \frac{1}{\tau_{21}} + \frac{G_d(1-\epsilon S_0)}{N_p}S_0 \quad (18e)$$

$$C_{24} = -\frac{G_d(1-\epsilon S_0)}{N_p}(N_{30}-N_{20}) \quad (18f)$$

$$C_{31} = -\frac{1}{\tau_{31}} \quad (18g)$$

$$C_{32} = -\frac{1}{\tau_{21}} \quad (18h)$$

$$C_{33} = j\omega + \frac{1}{\tau_{out}} \quad (18i)$$

$$C_{41} = -G_d(1-\epsilon S_0)S_0 \quad (18j)$$

$$C_{42} = G_d(1-\epsilon S_0)S_0 \quad (18k)$$

$$C_{44} = j\omega - G_d(1-\epsilon S_0)S_0(N_{30}-N_{20}) \quad (18l)$$

Where $C_{13} = C_{23} = C_{34} = C_{43} = 0$. The magnitude of the frequency response is then

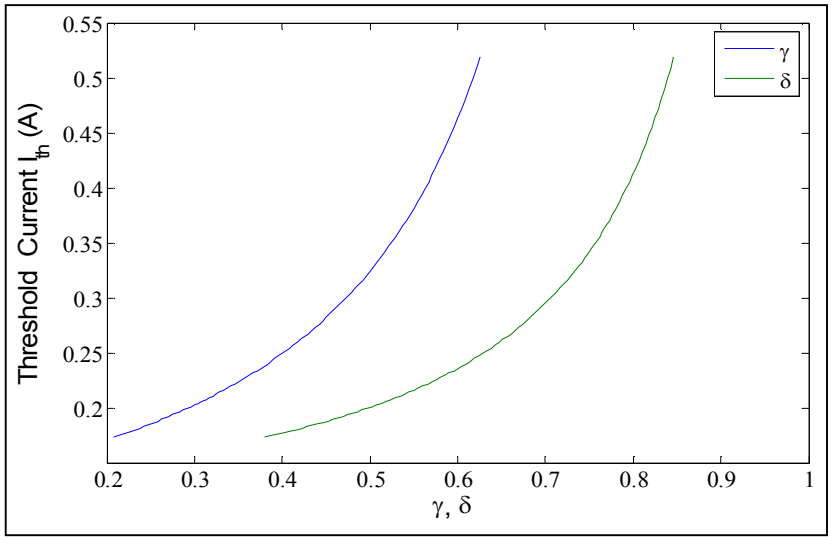


**Fig. 2.** $\delta = \delta = \tau_{21}/\tau_e (1 + \gamma)$ on the threshold injection current by the change of $\tau_{21}$ value when other parameters are constant.

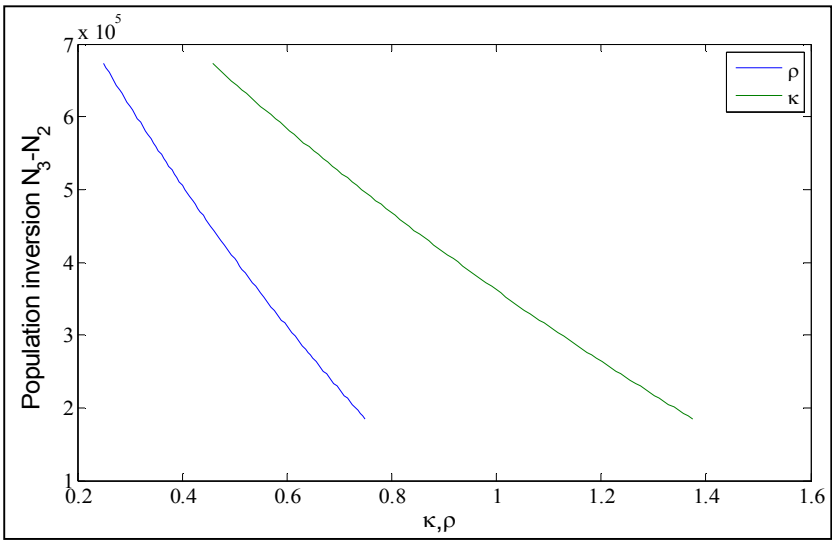


**Fig. 3.** The population inversion as a function of $\kappa = \tau_{21}/\tau_{32}$, $\rho = \tau_{21}/\tau_{\varepsilon}$.

$$H(\omega) = \frac{\omega_R^2}{\Delta} \quad (19) \qquad \omega_R^2 = \begin{vmatrix} A_{11} & A_{12} & A_{13} & A_{14} \\ A_{21} & A_{22} & A_{23} & A_{24} \\ A_{31} & A_{32} & A_{33} & A_{34} \\ A_{41} & A_{42} & A_{43} & A_{44} \end{vmatrix} \quad (20)$$

where

See appendix B for more details about the terms in Eq. (20).

$$\Delta = \begin{vmatrix} C_{11} & C_{12} & C_{13} & C_{14} \\ C_{21} & C_{22} & C_{23} & C_{24} \\ C_{31} & C_{32} & C_{33} & C_{34} \\ C_{41} & C_{42} & C_{43} & C_{44} \end{vmatrix} \tag{21}$$

## LANGEVIN RATE EQUATION MODEL

To derive an analytical equation for RIN, we must modify the three-level rate equation model to include the Langevin noise sources for carrier and photon as follows:

$$\frac{dN_3}{dt} = \eta\frac{I_{in}}{q} - \frac{N_3}{\tau_{32}} - \frac{N_3}{\tau_{31}} - \frac{G_d(1-\epsilon S)}{N_p}(N_3 - N_2)S + F_3 \tag{22}$$

$$\frac{dN_2}{dt} = \frac{N_3}{\tau_{32}} - \frac{N_2}{\tau_{21}} + \frac{G_d(1-\epsilon S)}{N_p}(N_3 - N_2)S + F_2 \tag{23}$$

$$\frac{dN_1}{dt} = \frac{N_3}{\tau_{31}} + \frac{N_2}{\tau_{21}} - \frac{N_1}{\tau_{out}} + F_1 \tag{24}$$

$$\frac{dS}{dt} = G_d(1-\epsilon S)(N_3 - N_2)S + \frac{\beta N_3}{\tau_e} - \frac{S}{\tau_p} + F_s \tag{25}$$

The final term of each equation, $F_3(t)$, $F_2(t)$, $F_1(t)$ and $F_s(t)$, is the effect of Langevin noise sources. In the present paper, the Langevin noise sources are calculated based on the same procedure in Ref. [8] as a method to simplify the rigorous quantum description of noise in QCLs. RIN is coming from shot noise associated with the discrete random flow of particles (carrier/photon) into and out of the reservoirs. To evaluate the Langevin noise density $\langle F_i F_i \rangle$, we simply sum overall rates of particle flow into and out of the reservoir (i). Also, to determine cross-correlation strength $\langle F_i F_j \rangle$ between two reservoirs (i) and (j) we sum only over particle flow which affects both reservoirs simultaneously.

$$\langle SS \rangle = 2\left[G_d(1-\epsilon S_0)N_3 S + \frac{\beta N_3}{\tau_e}\right] \tag{26}$$

$$\langle N_2 N_2 \rangle = 2\left[\frac{G_d(1-\epsilon S_0)N_3 S}{N_p} + \frac{N_3}{\tau_{32}}\right] \tag{27}$$

$$\langle N_3 N_3 \rangle = 2\left[\frac{G_d(1-\epsilon S_0)N_3 S}{N_p} + \frac{N_3}{\tau_e}\right] \tag{28}$$

$$\langle N_3 S \rangle = -\left[\frac{G_d(1-\epsilon S_0)N_3 S}{N_p} - \frac{G_d(1-\epsilon S_0)N_2 S}{N_p} + \frac{\beta N_3}{\tau_e}\right] \tag{29}$$

$$\langle N_3 N_2 \rangle = -\left[-\frac{G_d(1-\epsilon S_0)N_2 S}{N_p} + \frac{G_d(1-\epsilon S_0)N_3 S}{N_p} + \frac{N_3}{\tau_{32}}\right] \tag{30}$$

$$\langle N_2 S \rangle = -\left[\frac{G_d(1-\epsilon S_0)N_2 S}{N_p} + \frac{G_d(1-\epsilon S_0)N_3 S}{N_p} + \frac{\beta N_3}{\tau_{32}}\right] \tag{31}$$

As in modulation response part, an expression for the RIN spectra can be derived by applying a small signal analysis of the rate equation by inserting Eqs. ((10)-(13) and (16)) in Eqs. ((22)-(25)) as follows:

$$\begin{vmatrix} C_{11} & C_{12} & C_{13} & C_{14} \\ C_{21} & C_{22} & C_{23} & C_{24} \\ C_{31} & C_{32} & C_{33} & C_{34} \\ C_{41} & C_{42} & C_{43} & C_{44} \end{vmatrix} \begin{vmatrix} \Delta n_3 \\ \Delta n_2 \\ \Delta n_1 \\ \Delta s \end{vmatrix} = \begin{vmatrix} F_3 \\ F_2 \\ F_1 \\ F_s \end{vmatrix} \tag{32}$$

Now, to calculate RIN, we begin with calculating the photon number fluctuations ($\Delta s$) as follows:

$$\Delta s = \frac{\begin{vmatrix} C_{11} & C_{12} & C_{13} & F_3 \\ C_{21} & C_{22} & C_{23} & F_2 \\ C_{31} & C_{32} & C_{33} & F_1 \\ C_{41} & C_{42} & C_{43} & F_s \end{vmatrix}}{\Delta} \tag{33}$$

Inserting Eq. (19) in Eq. (33), we obtain an equation to determine the photon number fluctuations dependent on the

calculation of IMR as follows:

$$\Delta s = \frac{H(\omega)}{\omega_R^2}[H_3(\omega)F_3 + H_2(\omega)F_2 + H_1(\omega)F_1 + H_s(\omega)F_s] \quad (34)$$

Where

$$H_3(\omega) = -C_{21}C_{32}C_{43} + C_{21}C_{33}C_{42} + C_{22}C_{31}C_{43} - C_{22}C_{33}C_{41} \quad (35a)$$

$$H_2(\omega) = C_{11}C_{32}C_{43} - C_{11}C_{33}C_{42} - C_{12}C_{31}C_{43} + C_{12}C_{33}C_{41} \quad (35b)$$

$$H_1(\omega) = C_{12}C_{21}C_{43} - C_{11}C_{22}C_{43} \quad (35c)$$

$$H_s(\omega) = C_{11}C_{22}C_{33} - C_{21}C_{12}C_{33} \quad (35d)$$

In term of spectral density of the noise accompanying the signal, the RIN per unit bandwidth Δf is defined as the ratio of the photon number fluctuations and the mean photon number s as follows:

$$\frac{(RIN)}{\Delta f} = \frac{S_P(\omega)}{S^2} = \frac{1}{S^2}\lim_{T\to\infty}\frac{1}{T}|\delta s(\omega)|^2 \quad (36)$$

$$\frac{(RIN)}{\Delta f} = \frac{|H(\omega)|^2}{(\omega_R^2)^2}\begin{bmatrix} 2D_{33}\,|H_3(\omega)|^2 + 2D_{22}\,|H_2(\omega)|^2 \\ +4D_{32}\,\mathrm{Re}\big(H_3(\omega)H_2(\omega)\big) + 2D_{ss}\,|H_s(\omega)|^2 \\ +4D_{3s}\,\mathrm{Re}(H_3(\omega)H_s(\omega)) + 4D_{2s}\,\mathrm{Re}(H_2(\omega)H_s(\omega)) \end{bmatrix} \quad (37)$$

## CALCULATED RESULTS AND DISCUSSION

In this section, we calculate IMR and RIN numerically as a function of frequency. We study the effects of carrier transport between states on the RIN behavior and IMR in QCLs. Reference to [2,4,8], the following parameters are used in the present simulation $\tau_{32}$ = 2 ps, $\tau_{31}$ = 2.4 ps, $\tau_{21}$ = 0.5 ps, $G_d = 3 \times 10^5$ $s^{-1}$, $n_{eff}$ = 3.27, η = 0.33, $L_P$ , is the length of one stage = 40.7 nm, $\Gamma_w$ = 0.33. The rate equation of carriers in each state and photon was calculated numerically to obtain its steady-state values. The strong effect of $\tau_{21}$ on the physical properties of QCLs is quite clear in Eqs. ((9), (14) and (15)). Figure 2, shows the effect of $\gamma = \tau_{21}/\tau_{31}$ and $\delta = \tau_{21}/\tau_e\,(1+\gamma)$ on the threshold injection current by the change of $\tau_{21}$ value when other parameters are constant.

The increase of the optical phonon emission rate $\tau_{21}$ leads to increase the threshold injection current to obtain high electron density in level 3 compared to the electron density in level 2. This problem can be solved by decrease the energy difference between level 2 and level 1. In mostly, the electron temperature in QCLs $T_e$ , higher than the lattice temperature and dependent linearly on the current injection density which is related to devices structures and energy states. Therefore, any increase in electron temperature because of the increase in threshold current density and to failure in run the QCLs devices at room temperature. Hence, it is necessary that the electron transport $\tau_{21}$ is in less value as possible. By following the same procedure in Ref. [8], the effect of the optical phonon emission rate $\tau_{21}$ on the population inversion and saturation photon density is obtained. Figure 3 shows the effect of $\kappa = \tau_{21}/\tau_{32}$, $\rho = \tau_{21}/\tau_\varepsilon$ on the population inversion $N_3$-$N_2$ in QCLs device, where $\tau_e = \tau_{32} + \tau_{31}/\tau_{32}\,\tau_{31}$

If the optical phonon emission rate $\tau_{32}$ is constant, the increase in optical phonon emission rate $\tau_{21}$ leads to decrease the factor (1-κ) and therefore decrease the population inversion $N_3$-$N_2$. If $\tau_{21} = \tau_{32}$, the population inversion $N_3$-$N_2$ equals to zero. If $\tau_{21} > \tau_{32}$, the population inversion $N_3$-$N_2$ will be to negative values and therefore the QCLs structure tends to absorb incoming photons. It is clear that, the small effect of ρ in comparison with the κ, because of the small value of $\tau_{21}$ in the present simulation which is equal to 0.5 ps. Figure 4 shows the effect of increase in $\gamma = \tau_{21}/\tau_{31}$ on the saturation photon density. In Fig. 4, the $S_s$ tends to decrease with increasing the value of $\tau_{21}$ especially with low injection current value. Therefore, to get good operation of QCLs at room temperature, the injection current must be increased to eliminate the effect of $\tau_{21}$. It should be noted that the optimum performance of QCLs is strongly related to the waveguide loss in and mirror loss and the gain coefficient.

Figure 5 shows the calculated RIN of a QCL as a function of the frequency for different values of $\tau_{31}$. In the present simulation, we assume that all other parameters in

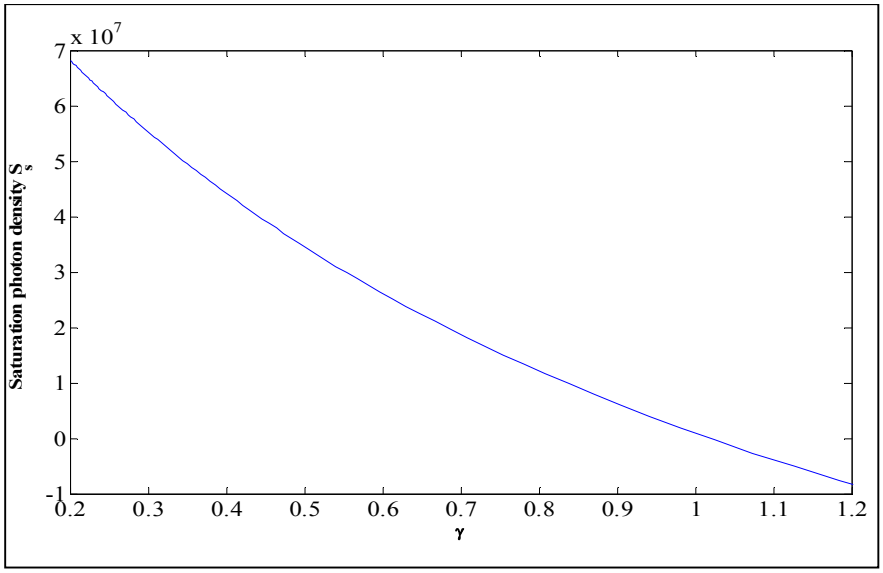


**Fig. 4.** The saturation photon density as a function of $\gamma = \tau_{21}/\tau_{31}$.

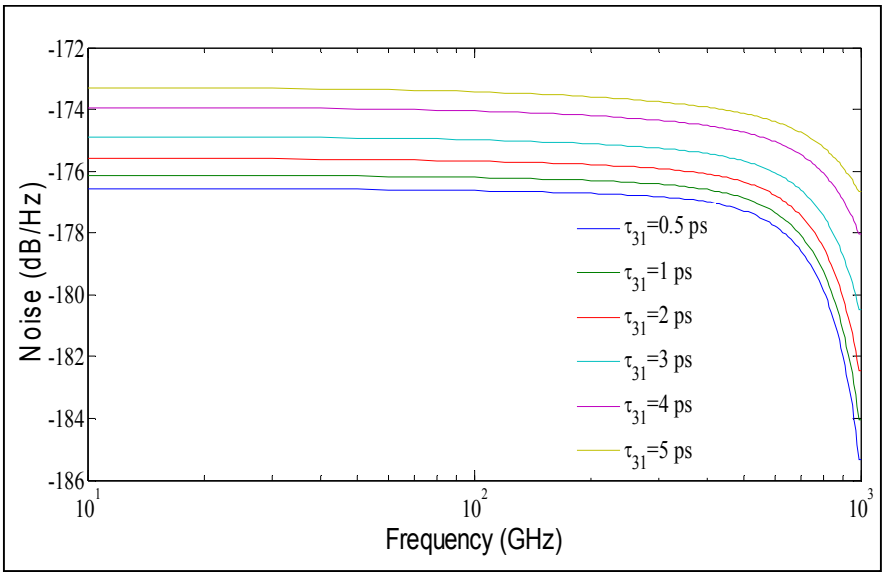


**Fig. 5.** Calculated RIN as a function of frequency at different values of $\tau_{31}$.

rate equations model are constant except $\tau_{31}$. In the present simulation, we assume that all other parameters in rate equation model are constant except ($\tau_{31}$) were assumed to be independent of the injection current. The RIN increases with increasing in $\tau_{31}$. The effect of $\tau_{31}$ is similar to that of $\tau_{21}$ where the increase in both times leads to decrease the population inversion and the output photons density. Therefore, it is necessary to operate QCLs at high injection current and the QCLs structure must be supported to improve fast electron transport time. Note that there is no

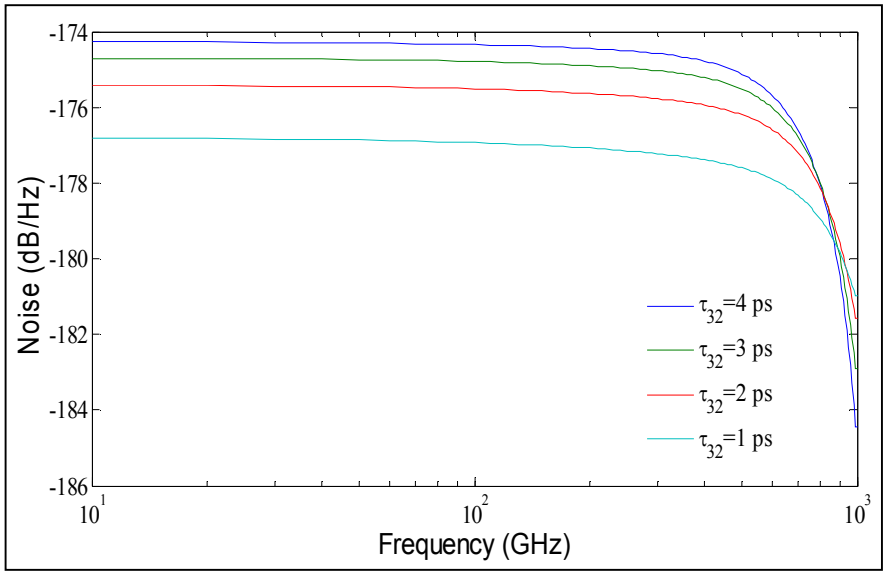


**Fig. 6.** The Calculated RIN as a function of frequency at different values of $\tau_{32}$.

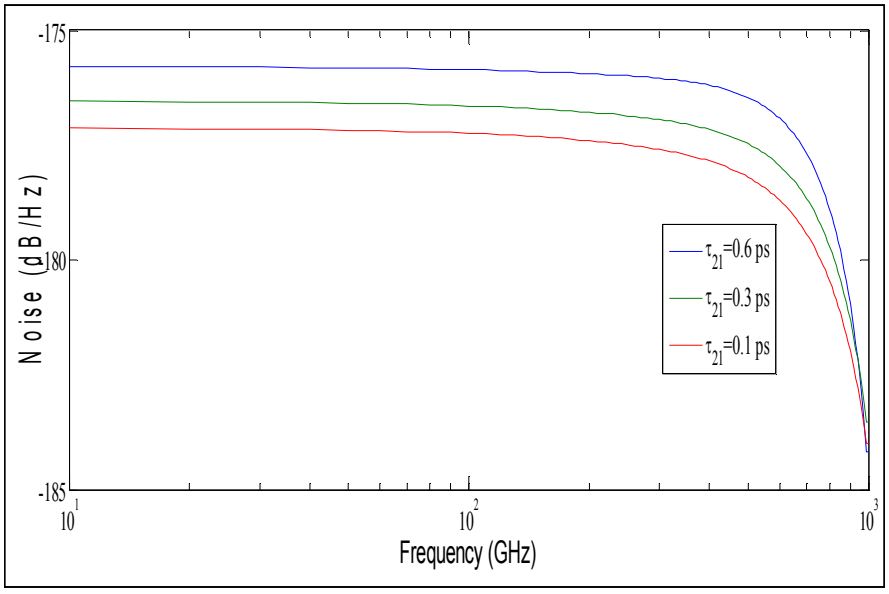


**Fig. 7.** Calculated RIN as a function of frequency at different values of $\tau_{21}$.

peak in noise spectrum and the white noise appears in the frequency range between (1-100) GHz. In quantum cascade lasers, $\tau_{21}$, $\tau_{32}$ and $\tau_{31}$, are dependent on two parameters; the energy difference between corresponding states and the phonon energy for carrier scattering. Therefore, any change in these parameters leads to change in these time transitions between states in QCLs.

Figure 6 shows the calculated intensity noise of a QCL

as a function of frequency for different values of $\tau_{32}$. In QCL, we can define the radiative efficiency $\eta_r$ as the ratio between the total numbers of electron injection per second in each gain period contributing to photon emission to the total electrons injected. The value of radiative efficiency is correlated with electron transport time. The increase in intensity noise because of the increase in $\tau_{32}$ is coming from the delay in electron transport leading to decrease the output photon density and, therefore, increase in noise values. When other parameters are constant, the increase in $\tau_{32}$ from 0.5 ps to 2 ps leads to decrease the population inversion from $16 \times 10^5$ to $2 \times 10^5$ and increase the threshold current from 0.2 A to 9 A for the same values of $\tau_{32}$. In general, the increase in $\tau_{32}$ leads to decrease the gain coefficient and the peak gain because of the strong coupling between the increase of $\tau_{32}$ and the static parameter of QCL. Therefore, the cavity length, lasing wavelength, and dipole matrix element must be improved to support the high values of gain coefficients.

Figure 7 shows the calculated intensity noise as a function of frequency for different values of $\tau_{21}$. Figures 8 and 9 shows the calculated intensity noise as a function of the frequency for different values of $\tau_p$ and a number of gain stage $N_p$ respectively. The increase in intensity noise in Fig 7, is accompanied by the low value of $\tau_{21}$ in comparison with high values of $\tau_{31}$ and $\tau_{32}$. In other words, the increase in $\tau_{21}$ even in small fractions leads to changes in noise behavior comparison with the large increase in other times such as $\tau_{31}$ and $\tau_{32}$. This result highlights the importance of improving $\tau_{21}$. In semiconductor lasers, the optical phonon emission rate is dependent on the energy differences between the energy levels. The photon lifetime is dependent on the structure parameters such as the refraction index, cavity length, the waveguide loss, mirror loss and the power reflectivity of the facets. The photon lifetime in QCLs is very close to the electron transport time. Therefore, the improvements in QCLs can be done with fast photon lifetime by using optimum device design parameters which result in small photon lifetime.

Finally, in Fig. 9, the RIN at different values of numbers of gain stages $N_p$. In noise behavior, the spectral density, material gain and total mode confinement factor scales linearly with the number of cascade stages. Therefore, with a small value of $N_p$, the main source of noise coming from the spontaneous emission but with a high value of $N_p$, the noise increases coming from the nonradioactive emission.

Figure 10 shows the calculated IMR of a QCL for different values of $\tau_{31}$, while all other parameters in rate equation model are constant except $\tau_{31}$. The effect of this time is very small at the lower frequencies, however, at higher frequencies where the operation of QCLs, any change in this time leads to increase in modulation bandwidth. The change in optical phonon emission rate in QCLs plays a critical role in the dynamics and static operation of QCLs where any change in this rate will affect the performance of these devices.

The radiative rate for spontaneous photon emission $\tau_{spont}$ in QCLs which is dependent on the energy of the electron at the states i and j. Any increase in the energy difference between states i and j, $E_{if}$, leads to decrease in the $\tau_{spont}$. While the optical phonon emission rate between any two states $\tau_{if}$ directly proportional to momentum between states $q_{if}$ which thus directly proportional to $E_{if}$. Therefore, it is expected that the effect of the change in these times will appear on the dynamic properties of QCLs of such modulation response and the efficiency of second harmonic generation. Figure 11 shows the calculated intensity modulation response of a QCLs for different values of $\tau_{32}$. The large effect of the change in optical phonon emission rate $\tau_{32}$ is the outcome of the direct dependence of the inverse population and $\tau_{32}$ in Eq. (10), where any delay in carrier transport leads to decrease the inverse population and increase the noise value. Figure 12 shows the calculated IMR for different values of $\tau_{21}$. It is clear that the increase in optical phonon emission rate has the large effect on the bandwidth value. In general, the modulation response of semiconductor lasers has a joint effect of each of the parasitic response and the intrinsic response as well.

In the present analysis, the effect of parasitic response is neglected, so all modulation response is dependent on the carrier-photon interaction and the gain medium. All effects of $\tau_{21}$ on IMR is based on the decrease of the inversion population and delay in transport relaxation time between gain stages in QCLs. Figure 13 shows the calculated IMR of a QCL for different values of photon lifetime $\tau_p$.

The photon lifetime value is approximately in the same magnitude of carrier lifetime, so the photon lifetime must be improved by using optimum parameters to QCLs structures.

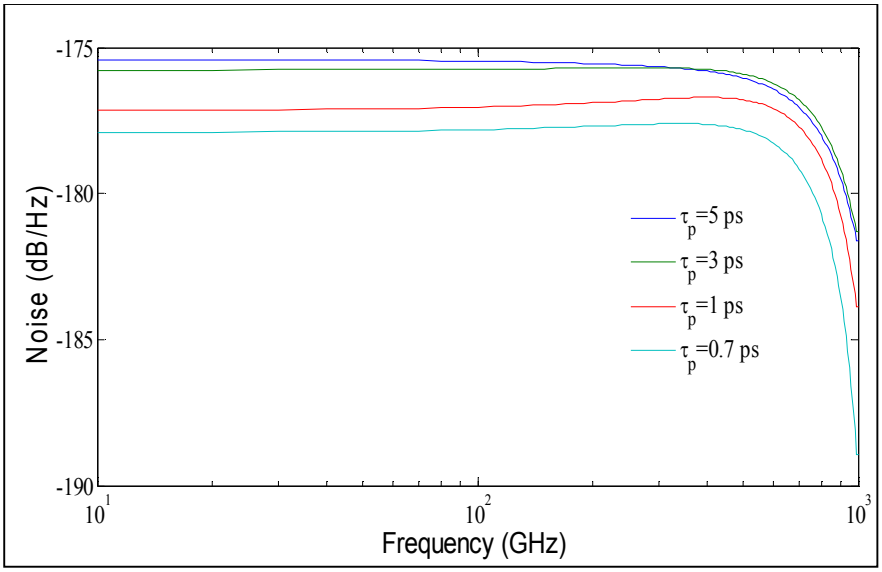


**Fig. 8.** Calculated RIN as a function of frequency at different values of $\tau_p$.

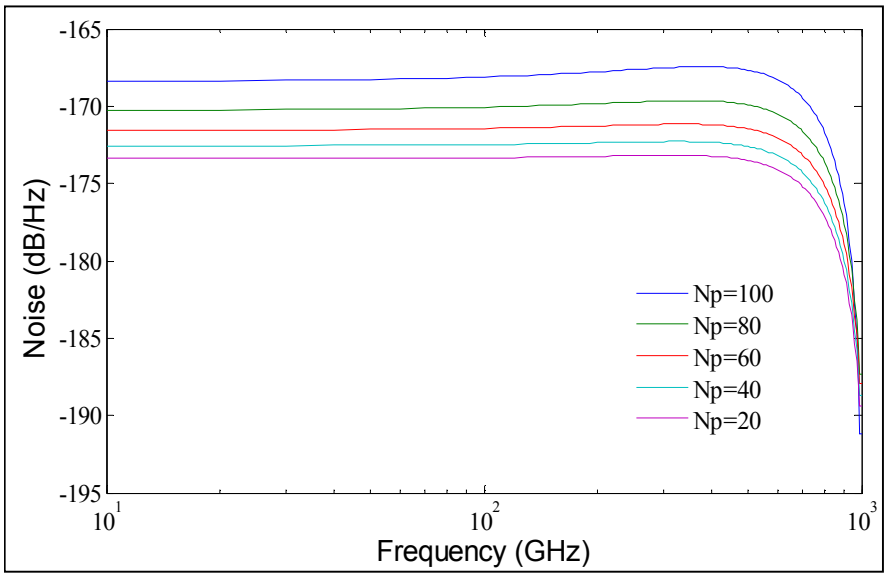


**Fig. 9.** The Calculated RIN as a function of frequency at different values of $N_p$.

Figure 14 shows the calculated IMR of a QCL for different values of $N_p$.

The effect of the increase in the number of gain stages is the same in intensity modulation response intensity noise behavior. The increase in gain stages leads to decrease the modulation bandwidth and increase the noise level. The increase in gain stages leads to decrease in the modulation bandwidth, where with increase the gain stage number the nonradiative transition is stronger efficient from the spontaneous emission. Whereas, with decrease the number

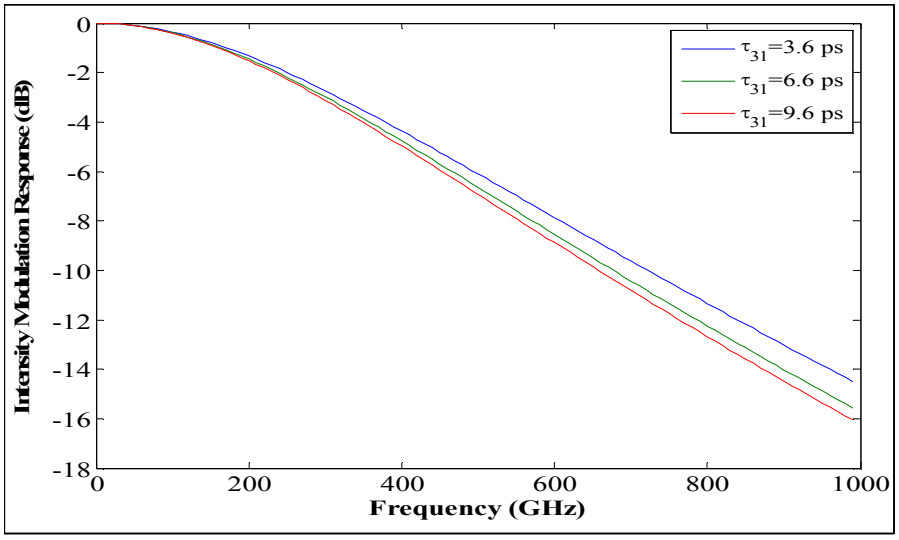


**Fig. 10.** Calculated IMR as a function of the frequency at different values of $\tau_{31}$.

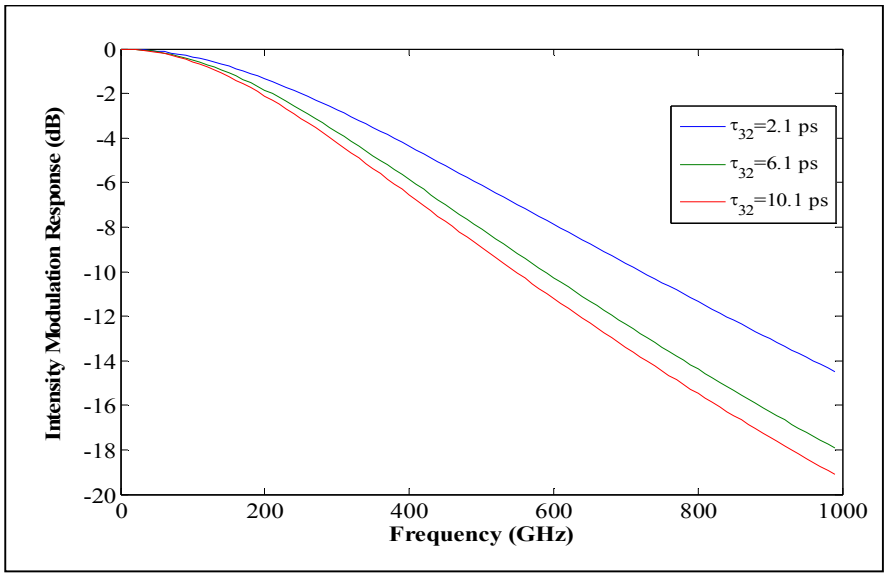


**Fig. 11.** Calculated IMR as a function of frequency at different values of $\tau_{32}$.

of gain stages, the spontaneous emission becomes more dominant. Finally, Fig. 15 shows the calculated IMR of a QCL as a function of the frequency for different values of $G_d$.

The optimum value of the gain coefficient is more intimately with the optimum value of the energy difference $E_{if}$, cavity length, full width at half maximum of the electroluminescence spectrum below the threshold, dipole matrix element, injection current, and inverse population. The increase in gain value means a decrease in all loss contributions that resulting from the device structures, carrier-photon interaction and gain medium. Tables 1 and 2,

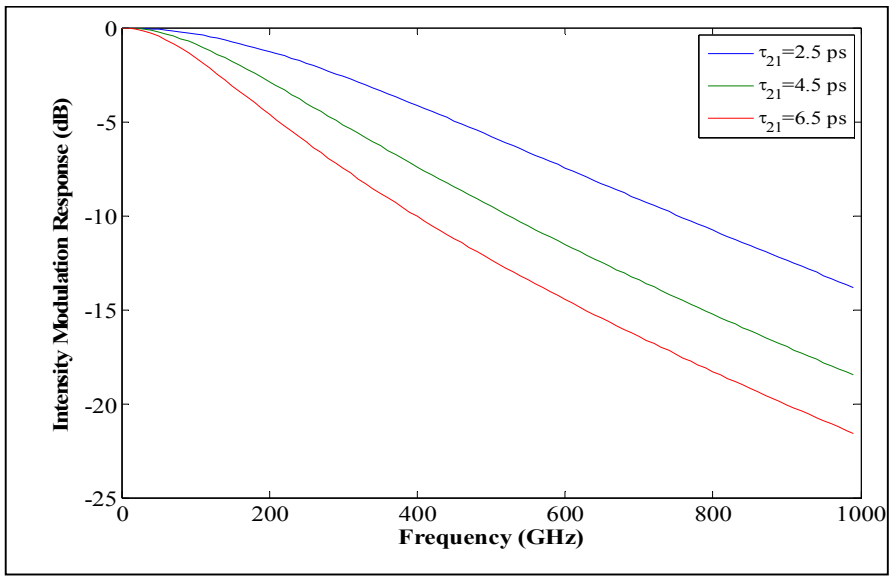


**Fig. 12.** Calculated IMR as a function of the frequency at different values of $\tau_{21}$.

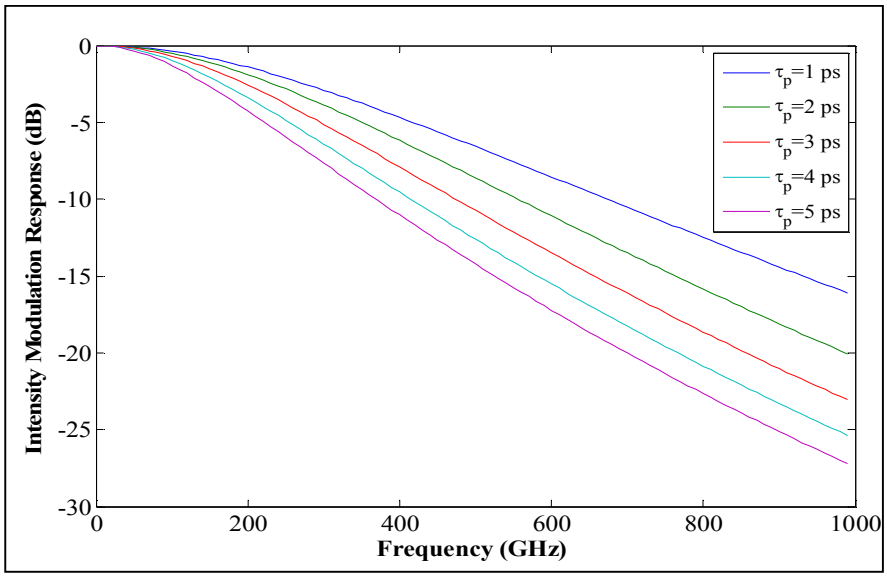


**Fig. 13.** Calculated IMR as a function of frequency at different values of $\tau_p$.

contain the optimum results of RIN and IMR obtained in the present results and previous experimental and theoretical works.

The results in the present work is dependent on the carrier dynamics in the rate equation model without any change in other parameters such as the injection current as in Ref. [11] or the well width as in Ref. [3]. For example, for slow carrier removal rates the modulation bandwidth in

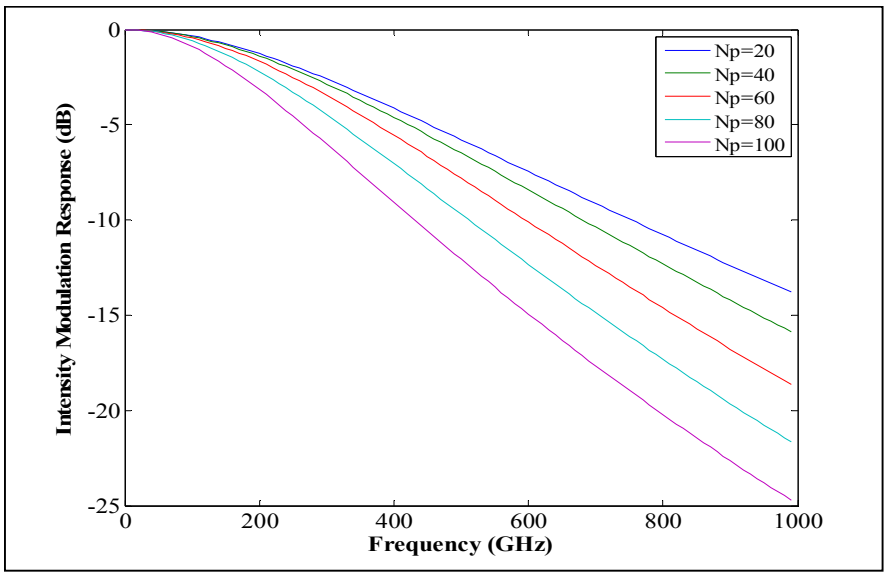


**Fig. 14.** Calculated IMR as a function of the frequency at different values of $N_p$.

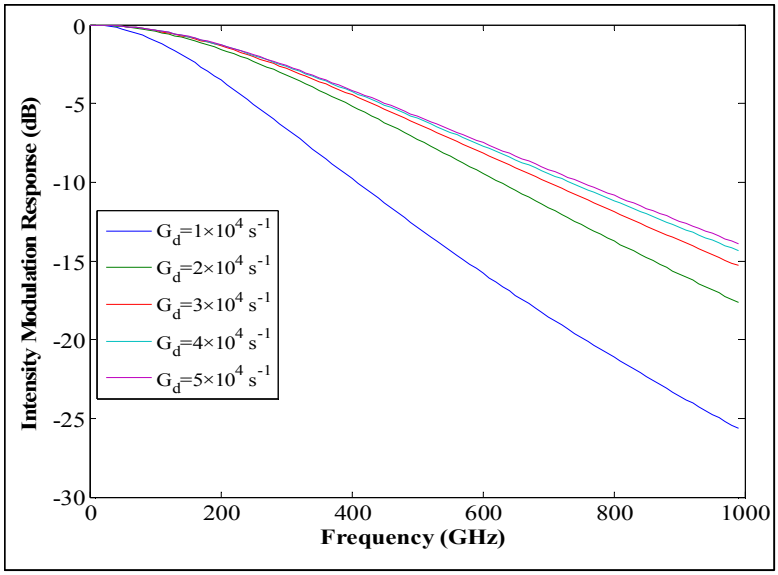


**Fig. 15.** Calculated IMR as a function of frequency at different values of $G_d$.

Ref. [11] is obtained with increase the injection current while if we talk about RIN in Ref. [3] the results have been calculated with rate equation model dependent on the well width. The large well width leads to decrease the energy difference between the energy states. Therefore the carrier dynamics represented in carrier lifetimes of rate equation model plays an important role in simulation process to investigate the properties of optoelectronic devices.

## CONCLUSIONS

In conclusion, based on rate equation model, we have

**Table 1.** RIN Values

| | RIN min. value (dB/Hz) | Ref. |
|---|---|---|
| Present work | -177 | |
| Mustafa *et al.* | -162 | [3] |
| Gensty and Elsaber | -175 | [8] |
| Experiential | -135 | [12] |

**Table 2.** IMR Values

| | IMR Bandwidth (GHz) | Ref. |
|---|---|---|
| Present work | 250 | |
| Cheung and Shore | 200 | [10] |
| Haldar | 800 | [11] |
| Experiential | 100 | [12] |

introduced analytical model for the relatively intensity noise (RIN) and intensity modulation response (IMR) in QCLs devices. Expressions for the RIN and IMR have been derived using small signal analysis of the rate equations. All transition lifetimes, photon lifetime, gain coefficient and number of gain stages were investigated in the present analysis. Mathematical analysis of the current study indicated that the optical phonon emission rate $\tau_{21}$ has strong effect on the (RIN) and (IMR). Moreover, the effect of $\tau_{21}$ is found to be higher in comparison with $\tau_{32}$, $\tau_{31}$ and the photon lifetime. So, the optical phonon emission rate $\tau_{21}$ must be improved to increase the modulation response bandwidth and decrease the noise value. In addition the increase in gain coefficient improves the (RIN) and (IMR) values. In this study, the rate equations model presented in the current study included many factors affecting on the noise properties and modulation behavior.

## APPENDIX A

In real semiconductor lasers, the steady state value means that the operation of device is fixed under constant input parameters such as injection current and input optical power and all other parameters in rate equation model. If we talk about the population inversion we write N30-$N_{20}$. On the other hand, changing any parameter in rate equation model leads to deviate the population inversion from steady state value; *i.e*, the steady state value of the population inversion is special case from the general case of the population inversion $N_3$-$N_2$.

From Eqs. ((5)-(8)) we have

$$\frac{N_{30}}{\tau_e} = \frac{\frac{\eta I_0}{q}\tau_{21}}{\tau_e(1+\frac{\tau_{21}}{\tau_{31}})} + \frac{\frac{1}{\tau_p G_d(1-\epsilon S_0)}}{\tau_e(1+\frac{\tau_{21}}{\tau_{31}})} \quad \text{(A1)}$$

From Eq. (8), the population inversion at threshold is given by

$$N_{30} - N_{20} = \frac{1}{\tau_p G_d(1-\epsilon S_0)} \quad \text{(A2)}$$

In substitution of Eq. (B2) in Eq. (B1) we get

$$\frac{N_{30}}{\tau_e} = \frac{\eta I_{th}\,\tau_{21}}{q\,\tau_e(1+\frac{\tau_{21}}{\tau_{31}})} + \frac{N_{30}-N_{20}}{\tau_e\left(1+\frac{\tau_{21}}{\tau_{31}}\right)} \tag{A3}$$

Substitution of Eq. (B3) in Eq. (5) yields

$$\frac{\eta I_{th}}{q} - \frac{\eta I_{th}\,\tau_{21}}{q\,\tau_e\left(1+\frac{\tau_{21}}{\tau_{31}}\right)} - \frac{N_{30}-N_{20}}{\tau_e\left(1+\frac{\tau_{21}}{\tau_{31}}\right)} - \frac{G_d(1-\epsilon S_0)}{N_p}(N_{30}-N_{20})S_0 = 0 \tag{A4}$$

Let

$$\delta = \frac{\tau_{21}}{\tau_e\left(1+\frac{\tau_{21}}{\tau_{31}}\right)}$$

We can re-write Eq. (B4) as follows:

$$\frac{\eta I_{th}}{q}(1-\delta) - \frac{N_{30}-N_{20}}{\tau_e\left(1+\frac{\tau_{21}}{\tau_{31}}\right)} - \frac{G_d(1-\epsilon S_0)}{N_p}(N_{30}-N_{20})S_0 = 0 \tag{A5}$$

Substitution of Eq. (B2) in Eq. (B5) yields

$$\frac{\eta I_{th}}{q}(1-\delta) = \frac{1}{\tau_p G_d(1-\epsilon S_0)\,\tau_e\left(1+\frac{\tau_{21}}{\tau_{31}}\right)} + \frac{S_0}{N_p\tau_p(1-\epsilon S_0)} \tag{A6}$$

In laser operation we have

$$\frac{1}{\tau_p G_d(1-\epsilon S)\,\tau_e\left(1+\frac{\tau_{21}}{\tau_{31}}\right)} \gg \frac{S_0}{N_P\tau_p(1-\epsilon S_0)}$$

Therefore we can neglect the second term in right side of the Eq. (B6) in following equations

$$I_{th} = \frac{q}{\eta\,\tau_p\tau_e G_d(1-\epsilon S)\left(1+\frac{\tau_{21}}{\tau_{31}}\right)(1-\delta)} \tag{A7}$$

To calculate $S_0$, from Eqs. ((B2) and (B4)) we have

$$\frac{\eta I_{th}}{q}(1-\delta) - \frac{1}{\tau_p G_d(1-\epsilon S)\,\tau_e\left(1+\frac{\tau_{21}}{\tau_{31}}\right)} - \frac{G_d(1-\epsilon S)}{N_p} S_0 \frac{1}{\tau_p G_d(1-\epsilon S)} = 0 \tag{A8}$$

Also, we can neglect the second term in right side of the Eq. (B8), and after a few steps we get

$$S_0 = \frac{\left(\frac{I}{I_{th}}-1\right)}{\tau_e\,G_0(1-\epsilon S)\left(1+\frac{\tau_{21}}{\tau_{31}}\right)} \tag{A9}$$

## APPENDIX B

In Eq. (20), we have the following constants:

| | | | |
|---|---|---|---|
| $A_{11} = \frac{1}{\tau_{32}} - \frac{1}{\tau_{31}} - \frac{G_d(1-\epsilon S_0)}{N_p} S_0$ | $A_{12} = -\frac{G_d(1-\epsilon S_0)}{N_p} S_0$ | $A_{13} = 0$ | $A_{14} = \frac{G_d(1-\epsilon S_0)}{N_p}(N_{30}-N_{20})$ |
| $A_{21} = -\frac{1}{\tau_{32}} - \frac{G_d(1-\epsilon S_0)}{N_p} S_0$ | $A_{22} = \frac{1}{\tau_{21}} + \frac{G_d(1-\epsilon S_0)}{N_p} S_0$ | $A_{23} = 0$ | $A_{24} = -\frac{G_d(1-\epsilon S_0)}{N_p}(N_{30}-N_{20})$ |

| | | | |
|---|---|---|---|
| $A_{31} = -\frac{1}{\tau_{31}}$ | $A_{32} = -\frac{1}{\tau_{21}}$ | $A_{33} = \frac{1}{\tau_{out}}$ | $A_{34} = 0$ |
| $A_{41} = -G_d(1-\epsilon S_0)S_0$ | $A_{42} = G_d(1-\epsilon S_0)S_0$ | $A_{43} = 0$ | $A_{44} = -G_d(1-\epsilon S_0)S_0(N_{30}-N_{20})$ |

## APPENDIX C

### Effects of Carrier Transport Time

I seek to demonstrate, how characteristic time constants including the photon lifetime and carrier intersubband transport time and other parameters in four-level rate equation model, determine the fundamental physical properties, IMR and RIN for QCLs devices. However, the state of population inversion ($N_3$-$N_2$) is a most important challenge for QCL devices, since optical-phonon emission is the dominant scattering mechanism between sub-bands whose energy separation is more than the optical-phonon energy. The optical-phonon emission leads to lifetimes of the order of picoseconds. Instead of a dipole matrix element, the optical transitions between the states are commonly described in terms of a dimensionless oscillator strength $f_{ij}$ defined by [13,14]:

$$f_{ij} = \frac{8\pi^2 m_0}{h^2}(E_{if})\langle\emptyset_i|Z|\emptyset_j\rangle^2 \tag{C1}$$

Also, the optical phonon-scattering ratio between any two states (i and f) is expressed by [15]:

$$\frac{1}{\tau_{if}} = \frac{2\pi^2 m^* \omega_{LO}}{h^2 \varepsilon_p q_{if}} \int dz \int dz' \, \emptyset_i(z)\emptyset_f(z) e^{-q_{if}(z-z')} \emptyset_i(z')\emptyset_f(z') \tag{C2}$$

where the momentum ($q_{if}$) is [14]:

$$q_{if} = \sqrt{\frac{8\pi^2 m^* (E_{if} - E_{LO})}{h^2}} \tag{C3}$$

where $m^*$ is the effective mass, $m_0$ is the electron mass, h is the Plank's constant, $E_{if}$ is the energy difference, $E_{LO}$ is the energy of the optical phonon and $\varepsilon_p$ is the permittivity. Therefore, the values of $f_{ij}$, $\tau_{if}$ and $q_{if}$ are dependent on the energy separation between associated states. For example, when we change the value $\tau_{21}$ , we suppose that the energy difference between states (2 and 1) changes due to changes in device structure [16] or changes in temperature due to applied bias [17,18] where other parameters are still constant, and when we change the value $\tau_{32}$, we suppose that the energy difference between states (3 and 2) changes where other parameters are still constant and so on.

The maximum modulation frequency is liable for optimization with respect to carrier transport time constants [10,17]. In turn, these provide further guidelines for the design of coupled quantum well structures to be utilized in QCLs. For this optimization, care must be taken to ensure that lifetimes are consistent with the conditions for population inversion. Therefore, I try to investigate the device operation with different carrier transport times due to applied bias, device structure and temperature.

## REFERENCES


[1] Murakami, A.; Kawashima, K.; Atsuki, K., Cavity resonance shift and bandwidth enhancement in semiconductor lasers with strong light injection. *J. Quan. Elec.,* **2003**, 39, 1196-1204, DOI: 10.1109/JQE.2003.817583.

[2] Lau, E.K.; Sung, H. K.; Wu, M.C., Frequency response enhancement of optical injection-locked lasers. *J. Quan. Elec.,* **2008**, 44, 90-99, DOI: 10.1109/JQE.2007.910450.

[3] Mustafa, N.; Pesquera, L.; Shore, K. A., Relative intensity noise of unipolar intersubband semiconductor lasers. *J. Mod. Opti.,* **2000**, *47*, 1825-1835, DOI: 10.1080/09500340008232435.

[4] Rana, F.; Ram R. J., Current noise and photon noise in quantum cascade lasers. *Phys. Revi. B,* **2002**. *65*, 1-29, DOI: 10.1103/PhysRevB.65.125313.

[5] Mustafa, N.; Pesquera, L.; Cheung, C. Y. L.; Shore, K. A., Terahertz bandwidth prediction for amplitude modulation response of unipolar intersubband semiconductor lasers. IEEE Phot. *Tech. Lett.,* **1999**. *11*, 527-529, DOI: 10.1109/68.759387.

[6] Lyakh, A.; Maulini, R.; Tsekoun, A.; Go, R.; Pflügl, C.; Diehl, L.; Wang, Q. J.; Capasso, F.; Kumar, C.; Patel, N., 3 W continuous-wave room temperature single-facet emission from quantum cascade lasers based on nonresonant extraction design approach. *App. Phys. Lett.* **2009**, *95*, 1-3, DOI: org/10.1063/1.3238263.

[7] Wang, Q. J.; Pflügl, C.; Diehl, L.; Capasso, F.; Edamura, T.; Furuta, S., Yamanishi, M.; Hirofumi, Kan., High performance quantum cascade lasers based on three-phonon-resonance design. *App. Phys. Lett.*, **2009**, *94*, 1-3, DOI: org/10.1063/1.3062981.

[8] Gensty, T.; Elsäßer, W., Semiclassical model for the relative intensity noise of intersubband quantum cascade lasers. *Opti. Com.,* **2005**, *256*, 171-183, DOI: 10.1016/j.optcom.2005.07.020.

[9] Cheung, C. Y. L.; Spencer, P. S.; Shore, K. A., Modulation bandwidth optimisation for unipolar intersubband semiconductor lasers. *IEE Proc. Opto.,* **1997**, *144*, 44-47, DOI: 10.1049/ip-opt:19971068.

[10] Cheung, C. Y. L.; Shore, K. A., Self-consistent analysis of the dc modulation response of unipolar semiconductor lasers. *J. of Mod. Opti.,* **1998**, *45*, 1219-1229, DOI: org/10.1080/09500349808230912.

[11] Haldar, M. K., A simplified analysis of direct intensity modulation of quantum cascade lasers. *IEEE J. Quan. Elec.,* **2005**, *41*, 1349-1355, DOI: 10.1109/JQE.2005.857062.

[12] Hercules, S.; Bogris, A.; Syvridis, D.; Elsasser, W., Intensity noise properties of mid-infrared injection locked quantum cascade lasers: I. Modeling. *IEEE J. Quan. Elec.* **2014**, *50*, 98-105, **DOI**: 10.1109/JQE.2013.2295434.

[13] Claude, W.; Vinter, B. Quantum semiconducte structures: Fundamentals and applications. Academ press, 2014.

[14] Helm, M., The basic physics of intersubbar transitions. Semiconductors and semimetals. 6 Elsevier, 1999.

[15] Ferreira, R.; Bastard, G., Evaluation of son scattering times for electrons in unbiased and biased single-and multiple-quantum-well structures. *Phys. Rev. B,* **1989**, *40*, 1074-1086, DOI: org/10.1103/ PhysRevB.40.1074.

[16] Cheung, C. Y. L.; Rees, P.; Shore, K. A., Gain calculations for unipolar semiconductor lasers. *IEE Proc. Opto.,* **1999**. *146*, 9-13, DOI: org/10.1049/ip-opt:19990452.

[17] Kalna, K.; Cheung, C. Y. L.; Shore, K. A., Electron transport process in quantum cascade intersubband semiconductor lasers. *J. App. Phys.,* 2001. *89*, **2001**-2005, DOI: org/10.1063/1.1339859.

[18] Cheung, C. Y. L.; Rees, P.; Shore, K. A.; Pierce I., Self-consistent optical gain and threshold current calculations for near infrared intersubband semiconductor lasers. *J. Mod. Opti.,* **2000**, *47*, 1857-1870, DOI: org/10.1080/09500340008232438.